AAAS
Research
Volume 2019, Article ID 8474698, 9 pages
https://doi.org/10.34133/2019/8474698

Research
OFFICIAL JOURNAL OF CAST

Research Article

Perovskite Solar Cells Yielding Reproducible Photovoltage of 1.20 V

Essa A. Alharbi[1], M. Ibrahim Dar[1,*], Neha Arora[1], Mohammad Hayal Alotaibi[2], Yahya A. Alzhrani[2], Pankaj Yadav[1], Wolfgang Tress[1], Ahmed Alyamani[3], Abdulrahman Albadri[3], Shaik M. Zakeeruddin[1], and Michael Grätzel[1]

[1]*Laboratory of Photonics and Interfaces, Institute of Chemical Sciences and Engineering, École Polytechnique Fédérale de Lausanne, Lausanne CH-1015, Switzerland*
[2]*National Nanotechnology Research Centre, King Abdulaziz City for Science and Technology (KACST), P.O. Box 6086, Riyadh 11442, Saudi Arabia*
[3]*National Center for Petrochemicals Technology, King Abdulaziz City for Science and Technology (KACST), P.O. Box 6086, 11442 Riyadh, Saudi Arabia*

[*]Correspondence should be addressed to M. Ibrahim Dar; ibrahim.dar@epfl.ch

Received 14 September 2018; Accepted 27 December 2018; Published 18 March 2019

Copyright © 2019 Essa A. Alharbi et al. Exclusive Licensee Science and Technology Review Publishing House. Distributed under a Creative Commons Attribution License (CC BY 4.0).

High photovoltages and power conversion efficiencies of perovskite solar cells (PSCs) can be realized by controlling the undesired nonradiative charge carrier recombination. Here, we introduce a judicious amount of guanidinium iodide into mixed-cation and mixed-halide perovskite films to suppress the parasitic charge carrier recombination, which enabled the fabrication of >20% efficient and operationally stable PSCs yielding reproducible photovoltage as high as 1.20 V. By introducing guanidinium iodide into the perovskite precursor solution, the bandgap of the resulting absorber material changed minimally; however, the nonradiative recombination diminished considerably as revealed by time-resolved photoluminescence and electroluminescence studies. Furthermore, using capacitance-frequency measurements, we were able to correlate the hysteresis features exhibited by the PSCs with interfacial charge accumulation. This study opens up a path to realize new record efficiencies for PSCs based on guanidinium iodide doped perovskite films.

1. Introduction

Over the past few years, perovskite solar cells (PSCs) have attracted great attention in the applied and theoretical research fields [1]. The appealing photophysical properties, such as small exciton binding energy, tunable bandgap, high absorption coefficient, relatively high carrier mobility and diffusivity, and tolerance to defects, broaden the application horizon of perovskites from photovoltaics to light emitting diodes and lasing [2–6]. Since PSCs were first introduced by the Miyasaka group in 2009, the power conversion efficiency (PCE) has been improved from 3.8% to over 23% using solution-based deposition methods [2, 7]. However, these methods can generate films exhibiting pinholes and defects, which are detrimental to the device performance due to the occurrence of parasitic charge carrier recombination under operational conditions [8, 9]. Therefore, to develop high-efficiency PSCs using solution-based approaches, one of the challenges is to achieve a rational control over the quality of the absorber layer [10, 11]. Recent reports on PSCs have shown that nonradiative charge carrier recombination or charge injection at the interfaces to charge transport layers limits the open circuit voltage (V_{OC}) [12–15]. The role of grain boundaries acting as recombination centers is under debate as such processes depend on the processing conditions and composition of the perovskite layer [16–20].

As it has become important to suppress the nonradiative recombination losses occurring at the interfaces or throughout the bulk of the perovskite film [21], many efforts have been devoted towards passivating the defects, which consequently retard the trap-assisted nonradiative charge carrier recombination. For example, a series of dialkylammonium and phenyltrimethylammonium halides were successfully explored to passivate the interfaces and grain boundaries

resulting in a much-improved PCE [22–24]. In a similar manner, the guanidinium (Gua) cation ($CH_6N_3^+$) was employed for the passivation of nonradiative recombination centers at $CH_3NH_3PbI_3$ grain boundaries enhancing the V_{OC} up to 1.07 V [25–27]. The Gua cation may also act as a cross-linker between the neighboring perovskite grains in the film [28]. It is worth emphasizing that the Gua cation was mainly investigated as an additive to $CH_3NH_3PbI_3$ based PSCs displaying moderate power conversion efficiencies. In addition to forming mixed-cation phases exhibiting relatively large bandgap, Gua cation can mix with MA and/or FA cations in the 3D perovskite lattice [29, 30] and consequently influence the excitonic and structural properties of the host phase remarkably. However, its influence on the bandgap, film quality, and performance of multication-based PSCs has not been explored so far.

In this article, we illustrate the effect of guanidinium iodide (GuaI) on the photophysical properties of mixed-cation and mixed-halide perovskite films. Thorough analyses based on scanning electron microscopy and emission studies were carried out to investigate the effect of GuaI addition on the morphology and emission of the perovskite material. Furthermore, electroluminescence and time-resolved photoluminescence studies were performed, respectively, to investigate the fully assembled devices and the charge carrier recombination occurring within the perovskite films. The operational stability carried out at a maximum power point under continuous full-sun illumination for 200 h showed that the PSCs containing Gua cations are as stable as control PSCs. In addition to providing new physical insights, we demonstrate for the first time robust stability for Gua based PSCs which are >20% efficient and yield photovoltage as high as 1.20 V.

2. Results

As a reference PSC, we used the mixed-halide and mixed-cation formulation "$Cs_{0.05}(MA_{0.17}\,FA_{0.83})_{0.95}Pb(I_{0.83}\,Br_{0.17})_3$" (abbreviated as Cs_5Pb). By adding x = 5% volume ratio of 1.5 M GuaI in DMSO, we prepared Cs_5Pb·*5*GuaI perovskite films [31].

2.1. Steady-State and Time-Resolved Photoluminescence. To unravel the impact of GuaI on the emission properties of the absorber layer, steady-state photoluminescence (PL) was measured for Cs_5Pb.*5*GuaI films (Figure 1(a)). Upon addition of 5% GuaI, a slight red shift from 757 to 766 nm in the peak position indicates that incorporation of GuaI in the perovskite lattice decreases the band gap slightly. In addition, the emission intensity enhanced dramatically with the incorporation of GuaI in Cs_5Pb precursor solution indicating a decrease in the nonradiative recombination.

Variation in the steady-state PL intensity apparently demonstrates that the level of defects promoting nonradiative carrier recombination in the perovskite film decreases upon introducing GuaI into the precursor solution. We employed time-resolved photoluminescence (TRPL) to further characterize the perovskite films quantitatively (Figure 1(b)). While exciting the films from the perovskite side using 408 nm photons, we studied the charge carrier dynamics occurring within the reference and $Cs_5Pb.x$GuaI perovskite films. Figure 1(b) shows that the incorporation of 5% GuaI dramatically increases the charge carrier lifetime. Charge carrier lifetime of 215 ns and 627 ns was estimated, respectively, for the Cs_5Pb, and $Cs_5Pb.0.05$GuaI films. The initial fast decay is strongly reduced in the $Cs_5Pb.0.05$GuaI film, consistent with the high PL intensity [32].

2.2. Morphological and Photovoltaic Characterization. Furthermore, the surface morphology of perovskite films was characterized via scanning electron microscopy (SEM) (Figure 2). Ostensibly, top view (Figures 2(a) and 2(b)) and cross-sectional (Figures 2(c) and 2(d)) SEM micrographs acquired from Cs_5Pb, $Cs_5Pb.0.05$GuaI perovskite films and the devices based on them confirm that the morphology of absorber layers is not affected by the addition of GuaI. The effect of GuaI incorporation on the photovoltaic performance is further examined in a device configuration of FTO/c-TiO_2/m-TiO_2/perovskite/spiro-OMeTAD/Au (for more details see Methods). Figure 3(a) depicts the *J-V* curves of the devices with 5% GuaI content in comparison to the reference Cs_5Pb device, and the corresponding photovoltaic parameters are summarized in Table 1. For the Cs_5Pb device, the highest PCE obtained is 20.03% with an open circuit voltage (V_{OC}) of 1.13 V, a short-circuit current density (J_{SC}) of 23 mA cm^{-2}, and a fill factor (FF) of 77%, which is in agreement with the values reported for the cesium-containing triple cation PSCs previously [31].

The PCE of $Cs_5Pb.0.05$GuaI based device is comparable to that of the reference device (Table 1). With respect to the Cs_5Pb based device, the $Cs_5Pb.0.05$GuaI devices showed higher J_{SC} values of 23.6 mA/cm^2. Intriguingly, the addition of 5% GuaI to Cs_5Pb significantly improved the V_{OC} from 1.13 V to 1.20 V. To the best of our knowledge, a V_{OC} of 1.20 V is among the highest values reported in the literature for a similarly configured PSC. Consistent with the PL data, Figure 3(b) shows the incident photon-to-current efficiency (IPCE) and integrated current density as a function of wavelength. From the IPCE spectra, we found that upon addition of 5% GuaI (Figure 3(b)), the same number of photons appears to generate more current compared to the reference Cs_5Pb device.

Based on the photovoltaic characterization, we found that the incorporation of 5% GuaI into mixed-cation and mixed-halide perovskite films improved the overall performance of PSCs. The reproducibility of the device performance was further ascertained by measuring 22 devices each from Cs_5Pb and $Cs_5Pb.0.05$GuaI as shown in Figure 3(c). We noted that a V_{OC} between 1.19-1.20 V is consistently achievable. By contrast, the fill factor of the $Cs_5Pb.0.05$GuaI devices is lower than that of the Cs_5Pb reference. Generally, the FF of a solar cell is affected by the series resistance (R_S) and ideality factor of the device [33]. By taking the slope of light *J-V* characteristics at the V_{OC}, R_S was calculated and summarized in Table S1. The $Cs_5Pb.0.05$GuaI device exhibits a higher value of R_S as compared to the Cs_5Pb device. Therefore, by

Table 1: Summarized J-V characteristics. J-V characteristics of the best devices with 5% GuaI content in comparison to the reference Cs_5Pb device.

Samples	J_{SC} (mA/cm^2)	V_{OC} (V)	FF (%)	PCE (%)
Cs_5Pb	23.0	1.13	77	20.0
Cs_5Pb.0.05GuaI	23.6	1.20	70	20.3

Table 2: Summarized electroluminescence data. Summary of the observed and calculated parameters derived from the electroluminescence data.

Device	V_{OC}, rad	EQE EL at injection current approx. J_{SC}	Nonrad. loss	V_{OC}, calc.
Cs_5Pb	1.34 V	0.09 %	180 mV	1.16 V
Cs_5Pb.0.05GuaI	1.34 V	0.3 %	150 mV	1.19 V

simply improving the FF, substantially higher PCEs could be realized.

2.3. Insight about the Hysteresis Behaviour. The Cs_5Pb and Cs_5Pb.0.05GuaI based devices were also examined for hysteresis (Figure S2) and despite favorable properties of Gua ions, such as zero dipole moment, the hysteresis effects were more prominent in GuaI based devices [34]. To understand the cause of the dominant hysteresis feature [35], capacitance-frequency measurements at zero bias in the dark were carried out (Figure 4(a)), where features in the low and high frequency of C-f response are clearly distinguishable. A constant capacitance element at a frequency >10^3 Hz for Cs_5Pb and >10^4 Hz for Cs_5Pb.0.05GuaI based devices is associated with the dielectric response of the absorber material. In turn, the capacitance in the low-frequency spectra could be associated with the ionic characteristics [35, 36]. Apparently, excess Gua ions, which are not confined within the perovskite crystal lattice and have weak bonding capability, could pile up near the contact interface and screen the local electric field leading to a higher value of capacitance in the low-frequency region [37]. By considering the electrostatic interactions at room temperature, space charge densities of 6.04×10^{17} cm^{-3} and 1.4×10^{18} cm^{-3} were obtained, respectively, for the reference and Cs_5Pb.0.05GuaI devices. The accumulation of relatively higher ions causes an excess capacitance in the low frequency, which consequently leads to the hysteresis. Furthermore, the motion of these ions under the applied bias can screen the internal electric field at the interface (TiO_2/perovskite), thus amplifying the hysteresis effect.

2.4. Electroluminescence Study. Electroluminescence (EL) measurements were carried out to compare the radiative emission properties of Cs_5Pb and Cs_5Pb.0.05GuaI PSCs. The EL was measured during a voltage sweep from 0 to 2 V and back. Figure S3 shows the *J-V* curve (solid lines) and emitted photon flux (dashed lines) obtained from Cs_5Pb and Cs_5Pb.0.05GuaI devices by a voltage loop starting from 0 V with a scan rate of 20 mV/s. The current onset is shifted towards higher voltages upon addition of GuaI (solid lines), consistent with the increased V_{OC}. This comes along with a roughly four-times higher radiative emission yield when compared at the same driving current (Figure 4(b)). Therefore, the increased PL signal and lifetime of charge carriers observed in perovskite films could be maintained. Following the approach in [38], V_{OC} can be derived from the emission yield (Table 2). The calculated values of 1.16 and 1.19 V for Cs_5Pb and Cs_5Pb.0.05GuaI, respectively, coincide with the experimental data.

2.5. Operational Stability of the Perovskite Solar Cells. Finally, the operational stability of Cs_5Pb and Cs_5Pb.0.05GuaI based devices was investigated at a maximum power point under constant one-sun illumination for 200 h in a nitrogen environment (Figure 4(c)) [39]. It is evident that Cs_5Pb and Cs_5Pb.0.05GuaI remain relatively stable for almost 200 h, which indicates that the incorporation of Gua cations, an organic species, does not introduce any additional source of degradation [40]. Thus far, such a promising operational stability has not been demonstrated for >20% efficient guanidinium-based PSCs yielding photovoltage as high as 1.20 V, which makes this investigation highly important.

3. Discussion

We investigated the effect of guanidinium iodide incorporation into mixed-cation and mixed-halides perovskite films. Apparently, a slight red shift from 757 to 766 nm in the PL peak position indicates the incorporation of GuaI in the perovskite lattice. A gradual increase in the content of GuaI shows a significant enhancement of the open circuit voltage from 1.13 V to 1.20 V leading to the realization of >20.3% PCE. The increased photoluminescence and lifetime of charge carriers observed in GuaI containing perovskite films were maintained in the fully assembled device, justifying the trends in the V_{OC}. PSCs containing a definite amount of GuaI showed four-times higher radiative emission yield than Cs_5Pb devices. The accumulation of higher ions in GuaI based PSCs causes an excess capacitance in the low-frequency response of capacitance-frequency measurements, which eventually increased the hysteresis. The realization of high photovoltages is quite intriguing, although while dealing with low FF values. Both parameters, i.e., V_{OC} and

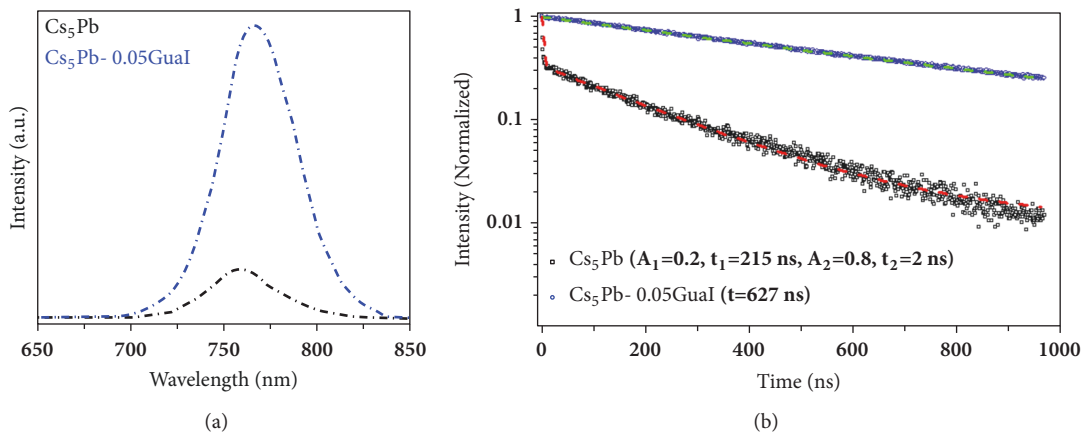


FIGURE 1: Photoluminescence studies of pure and GuaI containing perovskite films. (a) Steady-state photoluminescence, (b) time-resolved photoluminescence spectra; solid lines present the fitting curves obtained using a mono- or biexponential decay model.

FF, are interdepended as both are subservient to the ideality factor. Therefore, by simply improving the electronic and interfacial quality in the guanidinium iodide based perovskite systems, the FF values could be improved. Consequently, much higher photovoltages thus efficiencies exceeding record values can be achieved from the resulting perovskite solar cells. Finally, the thorough understanding gained through in-depth analyses unfolded the reasons leading to the realization of operationally stable and highly efficient (>20%) PSCs yielding photovoltage as high as 1.20 V. Our study shows that there is still plenty of room to improve PCE to new record levels by strategically manoeuvring the precursor chemistry.

4. Materials and Methods

4.1. Experimental Design. We aimed to fabricate highly reproducible and highly efficient perovskite solar cell yielding remarkable photovoltages by judiciously tailoring the photophysical properties of perovskite structures. In this direction, the following steps and detailed characterization techniques, including spectroscopy, scanning electron microscopy, X-ray diffraction, and other device characterization techniques, were employed.

4.2. Materials. All materials were purchased from Sigma-Aldrich and were used as received, unless stated otherwise.

4.3. Substrate Preparation. Fluorine-doped tin oxide (FTO)-glass substrates (TCO glass, NSG 10, Nippon sheet glass, Japan) were chemically etched using Zn powder and 4 M HCl and cleaned by ultrasonication in Hellmanex (2%, deionized water), rinsed thoroughly with deionized water and ethanol, and then treated with oxygen plasma for 15 min. A 30 nm blocking layer (TiO_2) was deposited on the cleaned FTO by spray pyrolysis at 450°C using a commercial titanium diisopropoxide bis(acetylacetonate) solution (75% in 2-propanol, Sigma-Aldrich) diluted in anhydrous ethanol (1:9, volume ratio) as precursor and oxygen as a carrier gas. A 150 nm mesoporous TiO_2 layer was deposited by spin coating a diluted paste (1:6 wt. ratio) (Dyesol 30NRD: ethanol) (4000 rpm, acceleration 2000 rpm for 20 s) onto the substrate containing TiO_2 compact layer and then sintered at 450°C for 30 min in dry air. For Li treatment of mesoporous TiO_2, 150 μL of LiTFSI solution in acetonitrile (10mg/mL, freshly prepared in an argon atmosphere) was spin coated (3000 rpm, acceleration 2000 rpm for 20 s) after a loading time of 10 s. Thereafter, Li treated substrates were sintered at 450°C for 30 min.

4.4. Deposition of Perovskite Films. The perovskite films were deposited using a single-step deposition method from the precursor solution containing FAI (1M), PbI_2 (1.1 M), MABr (0.2 M), and $PbBr_2$ (0.2 M) in anhydrous dimethylformamide/ dimethylsulphoxide (4:1 (volume ratio)). Thereafter, 5% of CsI (Acros 99.9%) (1.5 M DMSO) (1.5 M DMSO) was added to the perovskite precursor solution. The precursor solution was spin coated onto the mesoporous TiO_2 films in a two-step program at 1000 and 6000 r.p.m. for 10 and 30 s, respectively. During the second step, 130 μl of chlorobenzene was dropped on the spinning substrate 10 s prior the end of the program. This was followed by annealing the films at 100°C for 40 min. The device fabrication was carried out under controlled atmospheric conditions with humidity <2%. For completing the fabrication of devices, 2,2',7,7'-tetrakis(N,N-di-p-methoxyphenylamine)-9,9-spirobifluorene (spiro-OMeTAD, 60 mM in chlorobenzene), the HTM was doped with bis(trifluoromethylsulfonyl)imide lithium salt, tris(2-(1H-pyrazol-1-yl)-4-tert-butylpyridine)- cobalt(III) tris(bis(trifluoromethylsulfonyl) imide) (FK 209, from Dyenamo), and 4-tert-Butylpyridine in a molar ratios of 0.5, 0.05, and 3.3, respectively. Finally, ~75 nm gold (Au) layer was thermally evaporated.

4.5. Device Characterization. The current-voltage (J-V) characteristics of the perovskite devices were recorded with a digital source meter (Keithley model 2400, USA). A 450 W xenon lamp (Oriel, USA) was used as the light source for

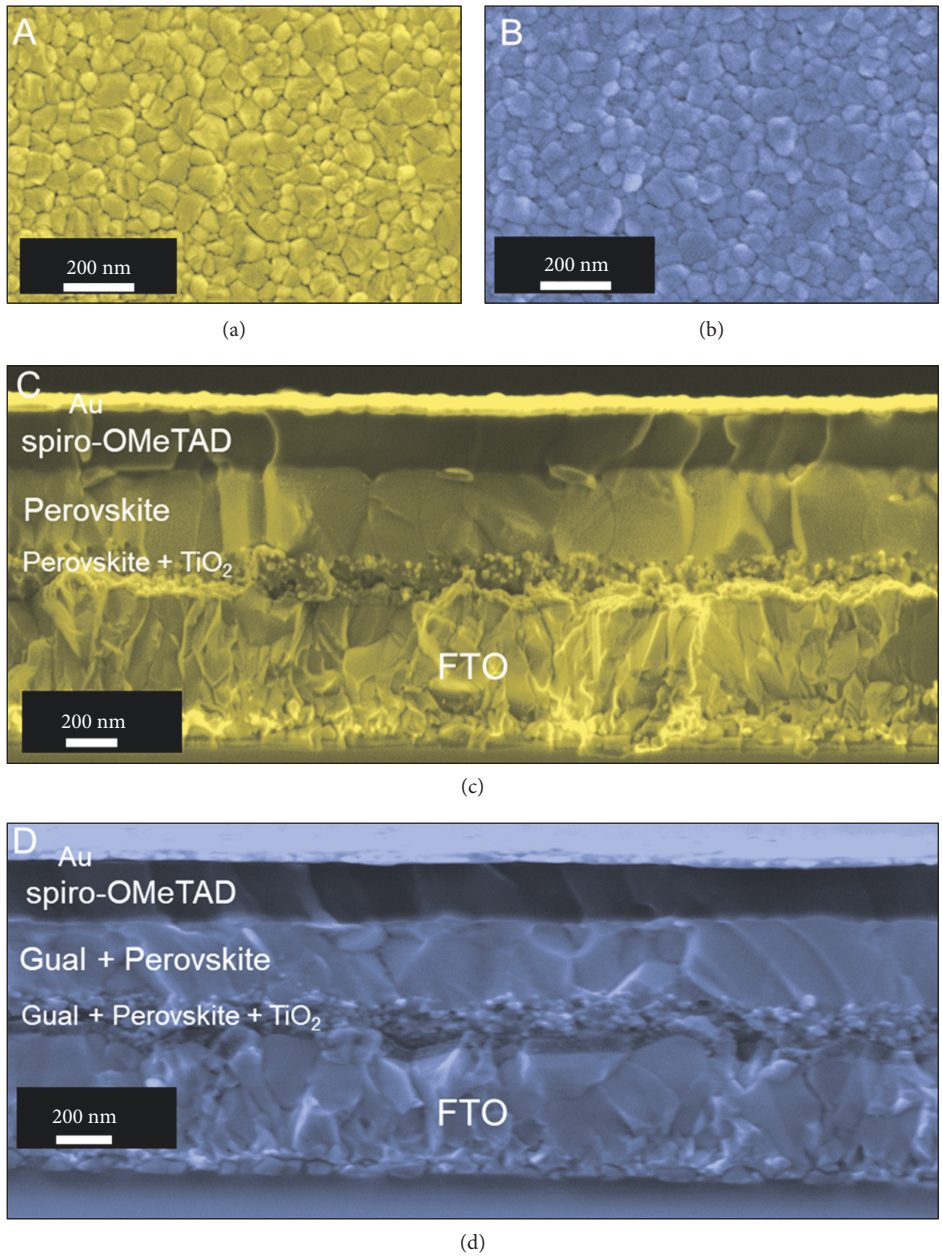


FIGURE 2: Morphological characterization. (a) and (b) Top view SEM micrographs acquired from Cs_5Pb, and $Cs_5Pb.0.05GuaI$ films. (c) and (d) Cross-sectional SEM micrographs acquired from the fully assembled devices based on Cs_5Pb and $Cs_5Pb.0.05GuaI$ films.

photovoltaic (J-V) measurements. The spectral output of the lamp was filtered using a Schott K113 Tempax sunlight filter (Präzisions Glas & Optik GmbH, Germany) to reduce the mismatch between the simulated and actual solar spectrum to less than 2%. The photo-active area of 0.16 cm^2 was defined using a dark-coloured metal mask. The IPCE measurements were performed using a LED light source (Ariadne EQE from Cicci Research).

4.6. Morphological Characterization. Scanning electron microscopy (SEM) was performed on a ZEISS Merlin HR-SEM using an In-lens detector.

4.7. Structural Characterization. X-ray diffraction data were collected on a Bruker Advance D8 X-ray diffractometer with a graphite monochromator, using Cu Kα radiation.

4.8. Spectroscopic Measurements. UV–vis measurements were performed on a Varian Cary 5. Photoluminescence spectra were obtained with a Florolog 322 (Horiba Jobin Ybon Ltd) in the wavelength range from 500 nm to 850 nm by exciting at 460 nm. The spectrometer working in a time-correlated single-photon counting mode with <ns time resolution was used for the time-resolved photoluminescence studies. Picosecond pulsed diode

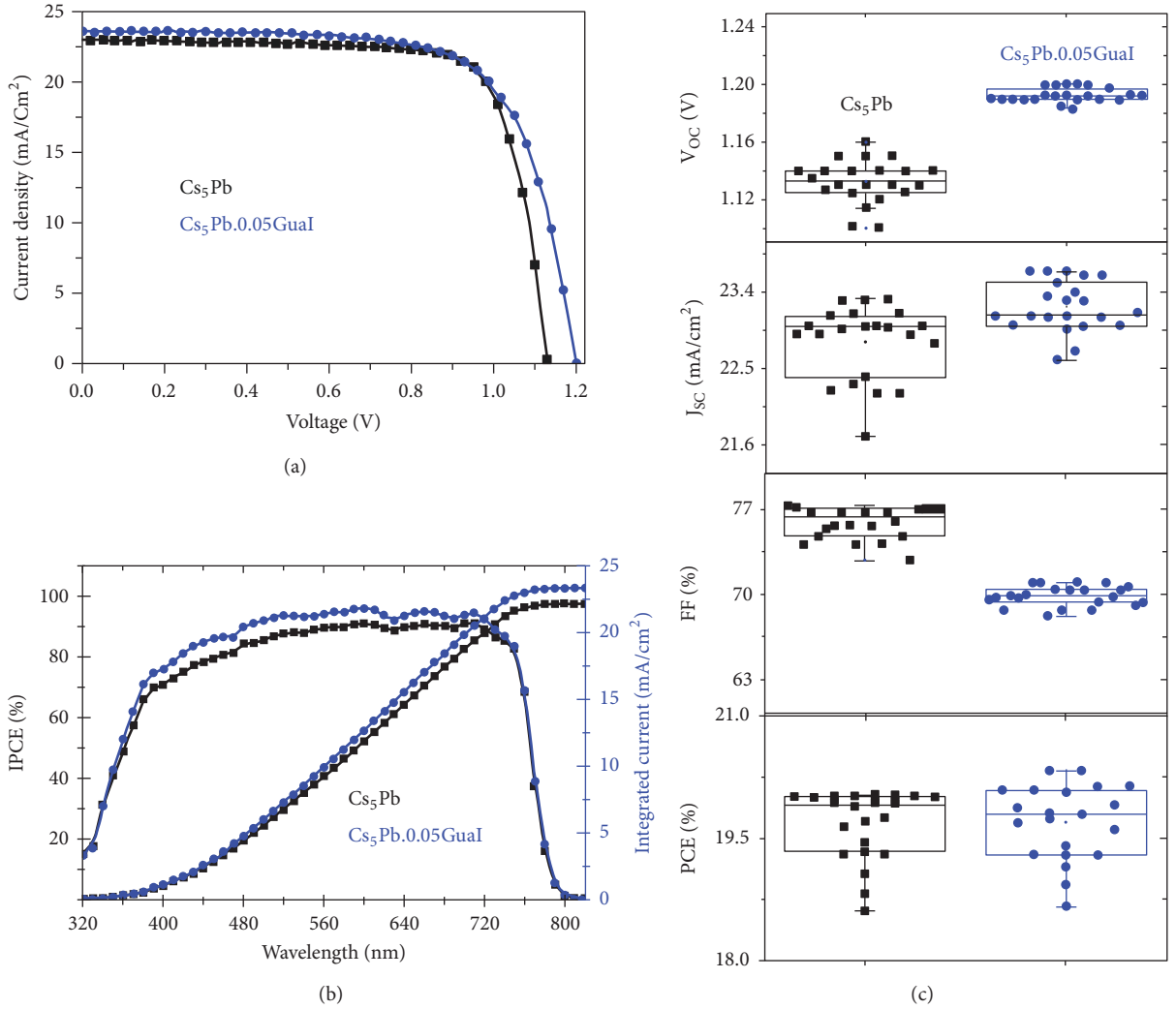


FIGURE 3: Photovoltaic characteristics of the perovskite solar cells based on Cs_5Pb and $Cs_5Pb.0.05GuaI$ films. (a) Current density versus voltage characteristics of perovskite solar cells. (b) Incident photon-to-current efficiency spectra as a function of the wavelength and the corresponding integrated J_{SC}. (c) J-V metrics for 22 devices using Cs_5Pb and $Cs_5Pb{\cdot}0.05GuaI$ films.

laser head NanoLED-405LH (Horiba) emitting <200 ps duration pulses at 408 nm with a repetition rate of 1 MHz was used as an excitation source.

4.9. Electroluminescence Measurements. The emitted photon flux was detected with a large-area (1 cm^2) Si-photodiode (Hamamatsu S1227-1010BQ) positioned close to the sample. The voltage scan was performed using a Bio-Logic SP300 potentiostat, which was also used to simultaneously measure the short-circuit current of the photodiode connected to a second channel.

4.10. Long-Term Light Soaking Test. Stability measurements were performed using a home-built system with white LED illumination with an intensity equivalent to 1 sun. The devices were kept at maximum power point (MPP) by a custom-made computer controlled MPP tracking routine. The inert atmosphere was achieved by flushing the sample holder with nitrogen.

Conflicts of Interest

The authors declare that there are no conflicts of interest regarding the publication of this article.

Authors' Contributions

M. Ibrahim Dar conceived and designed the project. Essa A. Alharbi, Neha Arora, and M. Ibrahim Dar recorded XRD, PL, and SEM data and characterized the devices. Essa A. Alharbi, M. Ibrahim Dar, Neha Arora, Mohammad Hayal Alotaibi, Yahya A. Alzhrani, and Shaik M. Zakeeruddin discussed, optimized, and fabricated the solar cells. Essa A. Alharbi recorded the stability measurements. Pankaj Yadav recorded and analyzed the capacitance versus frequency

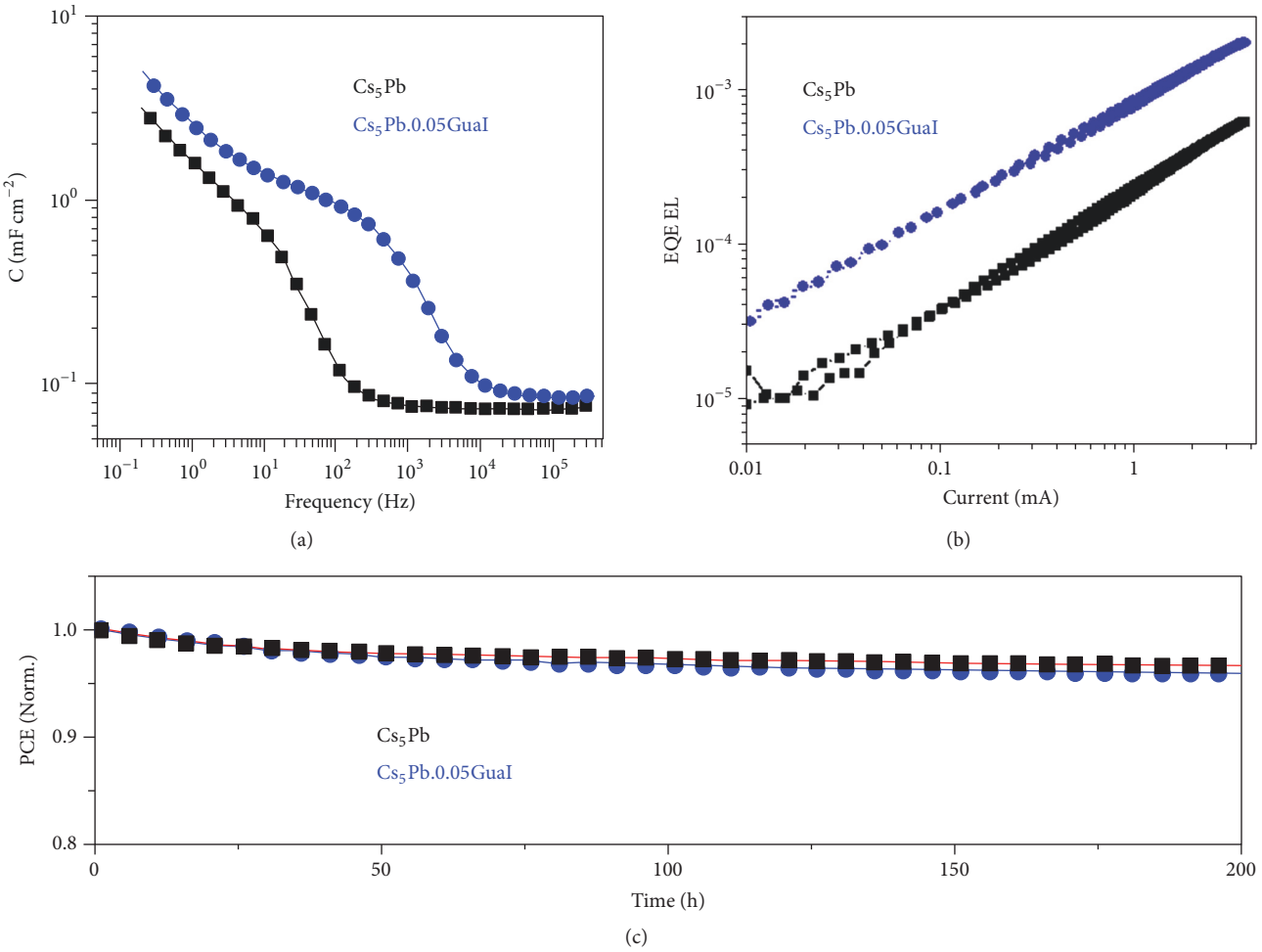


FIGURE 4: Electroluminescence and stability measurements. (a) Capacitance versus frequency spectra of Cs_5Pb and $Cs_5Pb.0.05GuaI$ based devices under short-circuit condition in the frequency range from 200 MHz to 1 MHz. The active area of perovskite solar cell is 0.16 cm^2 for both measurements. (b) External electroluminescence quantum efficiency as a function of the injection current for the Cs_5Pb and $Cs_5Pb.0.05GuaI$ devices. (c) A comparison of operational stability of Cs_5Pb and $Cs_5Pb.0.05GuaI$ devices. The devices were measured under a nitrogen environment at room temperature under constant illumination (LED source, approximated 1 Sun) at a maximum power point for 200 h.

spectra. Wolfgang Tress recorded and analyzed the EL data. Ahmed Alyamani and Abdulrahman Albadri contributed towards the analysis of PL and device characterization. M. Ibrahim Dar and Essa A. Alharbi wrote the manuscript and all the authors contributed towards finalizing the manuscript. Michael Grätzel directed and supervised the project. Essa A. Alharbi and M. Ibrahim Dar have contributed equally to the work.

Acknowledgments

Essa A. Alharbi gratefully acknowledges King Abdulaziz City for Science and Technology (KACST) for the fellowship. M. Ibrahim Dar acknowledges the financial support from the Swiss National Science Foundation under the project number P300P2_174471. M. Ibrahim Dar, Shaik M. Zakeeruddin, Wolfgang Tress, and Michael Grätzel thank the King Abdulaziz City for Science and Technology (KACST) for financial support. Neha Arora gratefully acknowledges financial support from Greatcell Solar.

Supplementary Materials

Figure S1. Photoluminescence spectra recorded from $Cs_5Pb.xGuaI$ films deposited onto the mesoporous Al_2O_3 substrate. Table S1. Summarized *J-V* characteristic of the devices with 5% GuaI content in comparison to the reference Cs_5Pb device. Figure S2. Forward and reverse current-voltage scans for (a) Cs_5Pb and (b) $Cs_5Pb.0.05GuaI$ devices. Figure S3. *J-V* curve (solid lines) and emitted photon flux (dashed lines) obtained from Cs_5Pb and $Cs_5Pb.0.05GuaI$ devices by a voltage loop starting from 0 V with a scan rate of 20 mV/s. Differences in current at low voltages are due to the hysteresis phenomenon. Figure S4. X-ray diffraction patterns corresponding to pure and GuaI containing perovskite films. *(Supplementary Materials)*

References

[1] C. C. Stoumpos, C. D. Malliakas, and M. G. Kanatzidis, "Semiconducting tin and lead iodide perovskites with organic cations: phase transitions, high mobilities, and near-infrared photoluminescent properties," *Inorganic Chemistry*, vol. 52, no. 15, pp. 9019–9038, 2013.

[2] A. Kojima, K. Teshima, Y. Shirai, and T. Miyasaka, "Organometal halide perovskites as visible-light sensitizers for photovoltaic cells," *Journal of the American Chemical Society*, vol. 131, no. 17, pp. 6050-6051, 2009.

[3] M. M. Lee, J. Teuscher, T. Miyasaka, T. N. Murakami, and H. J. Snaith, "Efficient hybrid solar cells based on meso-superstructured organometal halide perovskites," *Science*, vol. 338, no. 6107, pp. 643–647, 2012.

[4] H.-S. Kim, C.-R. Lee, J.-H. Im et al., "Lead iodide perovskite sensitized all-solid-state submicron thin film mesoscopic solar cell with efficiency exceeding 9%," *Scientific Reports*, vol. 2, article 591, 2012.

[5] H. Zhu, Y. Fu, F. Meng et al., "Lead halide perovskite nanowire lasers with low lasing thresholds and high quality factors," *Nature Materials*, vol. 14, no. 6, pp. 636–642, 2015.

[6] G. Xing, N. Mathews, S. S. Lim et al., "Low-temperature solution-processed wavelength-tunable perovskites for lasing," *Nature Materials*, vol. 13, no. 5, pp. 476–480, 2014.

[7] "NREL chart," https://www.nrel.gov/pv/assets/pdfs/pv-efficiency-chart.20181221.pdf.

[8] T. Leijtens, S. D. Stranks, G. E. Eperon et al., "Electronic properties of meso-superstructured and planar organometal halide perovskite films: Charge trapping, photodoping, and carrier mobility," *ACS Nano*, vol. 8, no. 7, pp. 7147–7155, 2014.

[9] M. I. Dar, A. Hinderhofer, G. Jacopin et al., "Function follows form: correlation between the growth and local emission of perovskite structures and the performance of solar cells," *Advanced Functional Materials*, vol. 27, no. 26, Article ID 1701433, 2017.

[10] D. Shi, V. Adinolfi, R. Comin et al., "Low trap-state density and long carrier diffusion in organolead trihalide perovskite single crystals," *Science*, vol. 347, no. 6221, pp. 519–522, 2015.

[11] H. D. Kim, H. Ohkita, H. Benten, and S. Ito, "Photovoltaic performance of perovskite solar cells with different grain sizes," *Advanced Materials*, vol. 28, no. 5, pp. 917–922, 2016.

[12] Y. Hou, W. Chen, D. Baran et al., "Overcoming the interface losses in planar heterojunction perovskite-based solar cells," *Advanced Materials*, vol. 28, no. 25, pp. 5112–5120, 2016.

[13] H. Chen, W. Fu, C. Huang et al., "Molecular engineered hole-extraction materials to enable dopant-free, efficient p-i-n perovskite solar cells," *Advanced Energy Materials*, vol. 7, no. 18, p. 1700012, 2017.

[14] J.-P. Correa-Baena, W. Tress, K. Domanski et al., "Identifying and suppressing interfacial recombination to achieve high open-circuit voltage in perovskite solar cells," *Energy & Environmental Science*, vol. 10, no. 5, pp. 1207–1212, 2017.

[15] N. Arora, M. I. Dar, M. Abdi-Jalebi et al., "Intrinsic and extrinsic stability of formamidinium lead bromide perovskite solar cells yielding high photovoltage," *Nano Letters*, vol. 16, no. 11, pp. 7155–7162, 2016.

[16] M. L. Agiorgousis, Y.-Y. Sun, H. Zeng, and S. Zhang, "Strong covalency-induced recombination centers in perovskite solar cell material $CH_3NH_3PbI_3$," *Journal of the American Chemical Society*, vol. 136, no. 41, pp. 14570–14575, 2014.

[17] D. W. de Quilettes, S. M. Vorpahl, S. D. Stranks et al., "Impact of microstructure on local carrier lifetime in perovskite solar cells," *Science*, vol. 348, no. 6235, pp. 683–686, 2015.

[18] J. S. Manser, J. A. Christians, and P. V. Kamat, "Intriguing optoelectronic properties of metal halide perovskites," *Chemical Reviews*, vol. 116, no. 21, pp. 12956–13008, 2016.

[19] M. Yang, Y. Zeng, Z. Li et al., "Do grain boundaries dominate non-radiative recombination in $CH_3NH_3PbI_3$ perovskite thin films?" *Physical Chemistry Chemical Physics*, vol. 19, no. 7, pp. 5043–5050, 2017.

[20] V. D'Innocenzo, A. R. Srimath Kandada, M. De Bastiani, M. Gandini, and A. Petrozza, "Tuning the light emission properties by band gap engineering in hybrid lead halide perovskite," *Journal of the American Chemical Society*, vol. 136, no. 51, pp. 17730–17733, 2014.

[21] S. D. Stranks, V. M. Burlakov, T. Leijtens, J. M. Ball, A. Goriely, and H. J. Snaith, "Recombination kinetics in organic-inorganic perovskites: excitons, free charge, and subgap states," *Physical Review Applied*, vol. 2, no. 3, Article ID 034007, 2014.

[22] X. Li, M. Ibrahim Dar, C. Yi et al., "Improved performance and stability of perovskite solar cells by crystal crosslinking with alkylphosphonic acid ω -ammonium chlorides," *Nature Chemistry*, vol. 7, no. 9, pp. 703–711, 2015.

[23] A. Abate, M. Saliba, D. J. Hollman et al., "Supramolecular halogen bond passivation of organic-inorganic halide perovskite solar cells," *Nano Letters*, vol. 14, no. 6, pp. 3247–3254, 2014.

[24] Y. Wang, T. Zhang, M. Kan, and Y. Zhao, "Bifunctional stabilization of all-inorganic α-CsPbI3 perovskite for 17% efficiency photovoltaics," *Journal of the American Chemical Society*, vol. 140, no. 39, pp. 12345–12348, 2018.

[25] N. D. Marco, H. Zhou, Q. Chen et al., "Guanidinium: a route to enhanced carrier lifetime and open-circuit voltage in hybrid perovskite solar cells," *Nano Letters*, vol. 16, no. 2, pp. 1009–1016, 2016.

[26] G. Giorgi, J.-I. Fujisawa, H. Segawa, and K. Yamashita, "Organic - Inorganic hybrid lead iodide perovskite featuring zero dipole moment guanidinium cations: A theoretical analysis," *The Journal of Physical Chemistry C*, vol. 119, no. 9, pp. 4694–4701, 2015.

[27] A. D. Jodlowski, C. Roldán-Carmona, G. Grancini et al., "Large guanidinium cation mixed with methylammonium in lead iodide perovskites for 19% efficient solar cells," *Nature Energy*, vol. 2, no. 12, pp. 972–979, 2017.

[28] X. Hou, Y. Hu, H. Liu et al., "Effect of guanidinium on mesoscopic perovskite solar cells," *Journal of Materials Chemistry A*, vol. 5, no. 1, pp. 73–78, 2017.

[29] D. J. Kubicki, D. Prochowicz, A. Hofstetter et al., "Formation of stable mixed guanidinium-methylammonium phases with exceptionally long carrier lifetimes for high-efficiency lead iodide-based perovskite photovoltaics," *Journal of the American Chemical Society*, vol. 140, no. 9, pp. 3345–3351, 2018.

[30] O. Nazarenko, M. R. Kotyrba, M. Wörle, E. Cuervo-Reyes, S. Yakunin, and M. V. Kovalenko, "Luminescent and photoconductive layered lead halide perovskite compounds comprising mixtures of cesium and guanidinium cations," *Inorganic Chemistry*, vol. 56, no. 19, pp. 11552–11564, 2017.

[31] N. Arora, M. I. Dar, A. Hinderhofer et al., "Perovskite solar cells with CuSCN hole extraction layers yield stabilized efficiencies greater than 20%," *Science*, vol. 358, no. 6364, pp. 768–771, 2017.

[32] M. I. Dar, G. Jacopin, S. Meloni et al., "Origin of unusual bandgap shift and dual emission in organic-inorganic lead

halide perovskites," *Science Advances*, vol. 2, no. 10, Article ID e1601156, 2016.

[33] P. Yadav, M. I. Dar, N. Arora et al., "The role of rubidium in multiple-cation-based high-efficiency perovskite solar cells," *Advanced Materials*, vol. 29, no. 40, Article ID 1701077, 2017.

[34] C. Eames, J. M. Frost, P. R. F. Barnes, B. C. O'Regan, A. Walsh, and M. S. Islam, "Ionic transport in hybrid lead iodide perovskite solar cells," *Nature Communications*, vol. 6, article 7497, 2015.

[35] E. L. Unger, E. T. Hoke, C. D. Bailie et al., "Hysteresis and transient behavior in current-voltage measurements of hybrid-perovskite absorber solar cells," *Energy & Environmental Science*, vol. 7, no. 11, pp. 3690–3698, 2014.

[36] I. Zarazua, J. Bisquert, and G. Garcia-Belmonte, "Light-induced space-charge accumulation zone as photovoltaic mechanism in perovskite solar cells," *The Journal of Physical Chemistry Letters*, vol. 7, no. 3, pp. 525–528, 2016.

[37] O. Almora, I. Zarazua, E. Mas-Marza, I. Mora-Sero, J. Bisquert, and G. Garcia-Belmonte, "Capacitive dark currents, hysteresis, and electrode polarization in lead halide perovskite solar cells," *The Journal of Physical Chemistry Letters*, vol. 6, no. 9, pp. 1645–1652, 2015.

[38] W. Tress, N. Marinova, O. Inganäs, M. K. Nazeeruddin, S. M. Zakeeruddin, and M. Graetzel, "Predicting the open-circuit voltage of $CH_3NH_3PbI_3$ perovskite solar cells using electroluminescence and photovoltaic quantum efficiency spectra: The role of radiative and non-radiative recombination," *Advanced Energy Materials*, vol. 5, no. 3, Article ID 1400812, 2014.

[39] H. Tan, A. Jain, O. Voznyy et al., "Efficient and stable solution-processed planar perovskite solar cells via contact passivation," *Science*, vol. 355, no. 6326, pp. 722–726, 2017.

[40] D. Bryant, N. Aristidou, S. Pont et al., "Light and oxygen induced degradation limits the operational stability of methylammonium lead triiodide perovskite solar cells," *Energy & Environmental Science*, vol. 9, no. 5, pp. 1655–1660, 2016.